Defects in heteroepitaxial structures studied with monoenergetic positrons: Large-lattice-mismatch systems Cu/Ag(111) and Ag/Cu(111)

P. A. Huttunen, J. Mäkinen, and A. Vehanen*
Laboratory of Physics, Helsinki University of Technology, SF-02150 Espoo 15, Finland
(Received 20 October 1989; revised manuscript received 15 December 1989)

In positron-beam experiments the backdiffusion probability of positrons is analyzed as a function of implantation energy to *nondestructively* extract depth distributions of open-volume defects in the near-surface region. We are reporting on the first quantitative studies of this type for metallic heteroepitaxial structures. Silver and copper layers have been grown on Cu(111) and Ag(111) substrates *in situ* under ultrahigh-vacuum conditions with an effusion-cell system. The overlayer thickness varies from 250 to 2800 Å. Epitaxial growth was confirmed with low-energy electron diffraction and Auger-electron spectroscopy measurements. Large lattice mismatch between silver and copper is expected to result in a large amount of lattice defects. In Cu/Ag(111) structures a vacancy concentration of the order of 1000 ppm or, alternatively, a dislocation density 1×10^{11} cm^{-2}, is observed near the interface. When silver is grown on Cu(111), the corresponding densities are smaller by a factor of 3. As the lattice constant of Cu is smaller than that of Ag, it is more likely that open volume defects exist in the Cu/Ag(111) system. The defect concentration reduces to half in both systems at the distance of $\sim$1000 Å, and the defect density decreases roughly exponentially as a function of distance from the interface.

I. INTRODUCTION

Wide use of layered structures in many technological applications has increased the need for basic knowledge on lattice matching between two different materials. There exist few methods which allow *nondestructive* studies of interfaces. Positrons are sensitive to the open-volume disorder inside a crystal due to their positive charge, which makes them a unique probe for vacancy-type defects. Monoenergetic positron beams have recently been used to study atomic scale defects on the surface and in the near-surface regions.[1] They have been utilized to yield information on sputtering[2] and ion implantation[3,4] induced defects as well as disorder associated with homoepitaxial crystal growth.[5] The first observations of positron trapping into defects in heteroepitaxial layered structures were reported by Schultz *et al.*[6] from Cu grown on W(110). In this paper we will extend the diffusion model to describe the motion of a thermal positron inside a heteroepitaxial structure and present the first quantitative experimental results from heteroepitaxial Cu/Ag(111) and Ag/Cu(111) structures. Preliminary results of this work were published in Ref. 7.

In many epitaxial systems, the crystal growth starts coherently with the lattice constant of the substrate.[8] At a critical thickness h_c it costs too much energy to strain additional layers into the coherence. The strain induced by the lattice mismatch begins to reduce from its maximum at h_c, and misfit dislocations are generated spontaneously. Misfit dislocations confined parallel to the interface reduce elastic strain effectively, and those having a component normal to the interface penetrate to the growing material. Misfit dislocations can be observed directly with electron microscopy.[9] X-ray diffraction has been used to provide information on misfit stress near the interface.[10] A technique giving complementary information to positrons is ion channeling, which is sensitive to the defects at interstitial sites.[11] These two methods have already been successfully combined in order to yield an overall picture of defects induced by proton implantation in silicon.[4] Recently Gidley has suggested the use of reemitted-positron spectroscopy (RPS) to determine the critical layer thickness h_c.[12]

The early stages of crystal growth have been widely characterized with different surface spectroscopies. Three different growth modes have been identified:[13] layer-by-layer growth, island growth, and Stranski-Krastanov (SK) growth, where 1 or more monolayers are formed prior to island formation. The silver and copper substrates used in this study are both fcc(111) single crystals, which have smooth close-packed surfaces. Another specific feature of the Cu/Ag system is the large difference in their lattice constants ($a_{Cu}=3.61$ Å and $a_{Ag}=4.09$ Å). Both systems have extensively been studied below 5 monolayers (ML) coverage. The growth of Cu on Ag(111) has been characterized by the electron-diffraction techniques,[14,15] the transmission-electron microscopy,[14] and the different electron spectroscopies.[15–18] The SK growth mode with one[15] or two[16,17] monolayers completing before three-dimensional islands are formed has been observed. In the connection of this work we found 1 monolayer SK growth.[19] Studies of the Ag/Cu(111) system at a low-coverage regime has been done with the electron-diffraction techniques,[20–23] the transmission-electron microscopy,[21–23] the different electron spectroscopies,[24–26,20] and the optical techniques.[25] The growth has been observed to be more ordered than in the opposite system. At least two epilayers are formed in registry with the Cu(111) substrate.[16,26,25,19] In thicker epitaxial structures, intermixing associated with the sample heating has been studied with Auger-electron spectroscopy (AES).[27] In polycrystalline materials, inter-

diffusion has been studied by Rutherford backscattering spectroscopy (RBS) (Ref. 28) and by depth profiling with ion-scattering spectroscopy (ISS) and AES.[29]

In considering the behavior of positrons implanted with keV energies, the layered structures can be divided into three classes. At coverages below 5 ML, the adsorbed atoms first change the surface dipole (<1 ML), and after that the interface potential difference for a positron evolves towards the affinity difference between the bulk materials. The observed changes in the signals given by positrons are mainly due to changes in the potential at the surface.[19] The layers of intermediate thickness (5–100 ML), where positron implantation to the overlayer still plays a minor role, provide a possibility to study the positron thermalization processes with monoenergetic positrons, as Gidley and Frieze have recently demonstrated.[30] A transport model used to extract mean free paths for different scattering channels from this data has recently been developed by Huttunen *et al.*[31] The interface potential has attained its final value (see Sec. III), and the surface branching of positrons starts to correspond to the overlayer material. Above 100 ML, positron implantation into the overlayer becomes significant, and the observed signals begin to yield the bulklike behavior of the layer material. The objective of this paper is to study these thickest structures, extracting information on the distribution of defects capable of trapping positrons in the overlayer. Results from thinner structures will be presented in a separate publication.[19]

We have made positron measurements from bilayered Cu/Ag(111) and Ag/Cu(111) structures from submonolayer coverages up to several-thousand-angstrom-thick layers. In the present paper we will concentrate on the thickness range between 250 and 2800 Å. In addition to the positron techniques, we have characterized samples with AES and low-energy electron diffraction (LEED). We have analyzed the backdiffusion probability measured from the structures grown by using an extended form of the diffusion model (see Appendix), which takes into account complications introduced by the interfacial potential. We are able to extract a defect profile for both systems, which shows that defect concentration is reduced roughly exponentially as the overlayer thickens. We note that the present extension to the diffusion model is only valid for structures (much) thicker than the mean free path for scattering from acoustic phonons (typically ~ 20 Å at room temperature).

The organization of the paper is as follows. Experimental conditions are reported in Sec. II. In Sec. III we present the extension to the diffusion model and discuss the interfacial potential. Experimental results are presented in Sec. IV, and in Sec. V we discuss the interpretation of these results. Section VI concludes the paper. In the Appendix the details of the diffusion model are summarized.

II. EXPERIMENTAL

A. Experimental environment

Experiments were done using a variable-energy positron beam, which has been described fully elsewhere.[32] Positrons from a ^{58}Co source enter a W(110) backscattering moderator. With an atomically clean and defect-free W(110) surface, we can extract a fraction of $\varepsilon = 0.30\%$ of the ^{58}Co β^+ activity to the monoenergetic positron beam (typically 10^6 e^+/s) striking the sample. The beam is guided to the sample chamber with a magnetic field. The energy of the beam ($\delta E \leq 3$ eV) can be adjusted from 1 eV up to 30 keV by floating the ^{58}Co source and the moderator area above the ground level. The beam diameter at the sample location is approximately 3 mm. The base pressure of sample chamber is 3×10^{-11} mbar as measured with a nude ionization gauge.

In Fig. 1 a schematic picture of the lower level of the two-level sample chamber is shown. Overlayers are evaporated with an effusion-cell system. Evaporants with a purity better than $6N$ are placed in a pyrolytic boron-nitride crucible. The crucibles are heated with a standard effusion cell which is efficiently surrounded by cooling water and liquid nitrogen. The material flow is controlled by a shutter, and its stability is checked with a water-cooled quartz-crystal thickness monitor. Additional shielding is used to minimize the contamination of the chamber. During the evaporations, the system pressure stays below 5×10^{-10} mbar. The layer thicknesses are determined with the quartz-crystal monitor calibrated with Auger spectroscopy. A relative accuracy of $\pm 20\%$ is achieved. Annihilations of positrons are detected with a high-purity Ge detector. The upper level is equipped with standard tools for surface treatment. It contains a sputter ion gun, a residual-gas analyzer (RGA), and a LEED–retarding-field-Auger (RFA) system for surface preparation and characterization.

B. Sample preparation

Several reasons influenced the choice of Cu and Ag as the materials in the present experiments. Noble metals have been extensively studied using bulk-positron experiments.[33] Large lattice mismatch between these materials

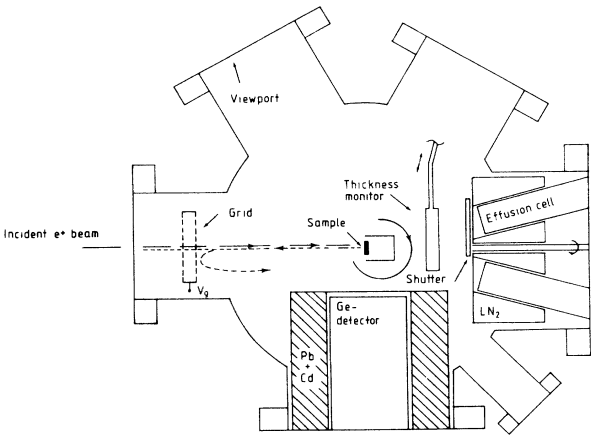

FIG. 1. Section of the sample chamber showing instrumentation for positron measurements and evaporations. Annihilation γ rays are detected with a Ge detector. Evaporations are done with an effusion cell system surrounded with a cryotrap. By biasing the grid, freely emitted positrons are either turned back to the sample or allowed to escape from the chamber (dashed line).

is expected to result in a large amount of lattice defects. Further, copper and silver are relatively easy to keep clean under UHV conditions.

The Ag(111) single crystal was obtained from Metal Crystals & Oxides Ltd., and it had a purity better than 99.999%. It was mechanically and electrolytically polished before installation in the chamber. The same treatments were applied to the Cu(111) crystals (>99.9999%) which were diamond-saw cut from a single crystal Cu rod.[34] The samples were cleaned *in situ* by subsequent Ar-ion etching and annealing cycles. Initially high Ar^+ energies (2–3 keV) were used to maximize the sputtering rate. The Ar^+ energy was gradually decreased down to 500 eV to minimize the sputter-induced damage remaining in the crystal.[2] The annealing temperatures were 700 °C for Ag and 800 °C for Cu. Cycles were repeated until LEED, AES, and positronium fraction measurements showed the characteristics of a clean defect-free surface. During the evaporations the sample was cleaned in the same way after each exposure. In order to minimize the danger of alloying, evaporated material was fully removed before raising the sample temperature. Prior to evaporations, the sample cleanliness was checked with AES, which showed <1% of a monolayer carbon and oxygen contamination.

The growth rate at the substrate is mainly determined by the vapor pressure of the evaporant, which can be adjusted by changing the oven temperature. In the present work temperatures between 900 and 1000 °C were used for Ag evaporations and 1000 and 1150 °C for Cu, depending on the desired layer thickness. The structures grown are listed in Table I, together with the growth rates. The layer thickness varied between 250 and 2800 Å and a typical growth rate was 10 Å/min. Substrates were usually held at room temperature during the growth. One 1175-Å-thick Ag/Cu(111) structure was grown with the substrate at 100 °C. Due to the interdiffusion at elevated temperatures,[27] the Cu/Ag system is not well suited for studies above room temperature.

C. Measured quantities

In the positron-beam experiments, energetic positrons are implanted into the solid. After thermalization, a certain fraction of them returns to the entrance surface. The motion of thermal positrons in solids is governed by scattering from acoustic phonons, and is normally described using a steady-state diffusion model.[35] By separating backdiffusing positrons from the other events, information on crystal quality between the implantation depth and surface can be obtained. In this work the backdiffusion probability $J(E)$ to the surface is determined from the relative fraction of positrons implanted with an energy E that are emitted as positronium (Ps) atoms. The incident positron energy is varied between 0 and 25 keV. The Ps fraction $f_+(E)$ is deduced from the annihilation photon spectrum by separating 3γ annihilations from 2γ events.[1] When two photons are emitted, each has an energy of ≈ 511 keV, whereas the spectrum from 3γ annihilations of Ps decay is continuous from 0 to 511 keV. The absolute fraction $f_+(E)$ can be determined from the ratio of events within the 511-keV annihilation peak to the total number of annihilation events.[1] When

TABLE I. Studied Cu/Ag(111) and Ag/Cu(111) structures. Parameter f_0 is obtained by direct extrapolation from the measured curve. Trapping rates κ_0 correspond to the defect fits where uniformly distributed defects in the overlayer are assumed. The accuracy in the thickness determination is ±20%. The asterisk indicates that growth was done on the substrate at 100 °C.

Sample		Thickness (Å)	Growth rate (Å/min)	f_0	κ_0(1/s)
Cu/Ag(111)	1	625(125)	6.5	0.345	1.2×10^{11}
		+200 °C anneal/5 min		0.390	6.2×10^{10}
	2	800(160)	11.2	0.345	1.4×10^{11}
		+200 °C anneal/5 min		0.420	5.9×10^{10}
	3	1135(230)	11.2	0.355	1.1×10^{11}
		+200 °C anneal/5 min		0.450	5.0×10^{10}
	4	2800(560)	11.2	0.365	3.8×10^{10}
Ag/Cu(111)	5	245(50)	13.8	0.465	3.9×10^{10}
	6	475(100)	13.8	0.45	4.8×10^{10}
	7	590(120)	13.8	0.45	3.4×10^{10}
	8	710(140)	13.8	0.45	2.5×10^{10}
	9	945(190)	13.8	0.43	3.2×10^{10}
	10	1175(240)	13.8	0.45	2.0×10^{10}
	11*	1175(240)	13.8	0.48	1.4×10^{10}
	12	1420(290)	13.8	0.455	1.7×10^{10}
Bulk Ag				0.48	
Bulk Cu				0.49	

$f_+(E)$ is measured, all free positrons emitted from a negative work-function[1] surface are returned to the target crystal by a positively biased grid. The measured signal thus has two different contributions: Ps which is formed in the primary emission process, and Ps which is formed from those positrons returned at least once to the crystal. The essential feature is that $f_+(E)$ is proportional to the backdiffusing current $J(E)$. This enables us the use of the diffusion model for data analysis (see Sec. III). Ps formation is strictly a surface process, since it is not possible inside a metal (see, e.g., Ref. 1). Of the surfaces used in this work, Cu(111) is a spontaneous positron emitter [i.e., it has a negative work function at 300 K $\phi_+^{\mathrm{Cu}(111)}=-0.33$ eV (Ref. 36)], while Ag(111) has a positive work function at 300 K [theoretically $\phi_+^{\mathrm{Ag}(111)}=0.6$ eV (Ref. 37)], and escape as free positrons is forbidden.

The defect distribution analysis has been made by fitting $J(E)$ curves, which have been calculated from

$$J(E)=f_+(E)/f_+(0)\ . \tag{1}$$

One of the main problems in determining the backdiffusing probability $J(E)$ is the proper evaluation of $f_+(0)$ corresponding to the Ps-formation branching ratio. At low incident energies a positron may escape prior to complete thermalization, which can be observed in either the fraction of positrons returning to the surface, or the energy dependence of the Ps-formation probability. When the diffusion model is applied to the measured data, these nonthermal processes can lead to uncertainties.[38–41] In this work $f_+(0)$ has been obtained by extrapolating directly from the measured curve, which leads to overestimates of the trapping rates for positrons, and therefore gives upper limits to defect concentrations. Epithermal positrons have been excluded from the analysis by neglecting data at the lowest energies, following the procedure used in positron-diffusion studies of defect-free single crystals.[40] This scheme enables a comparison of results from different samples.

In this work we did not follow the trapping fraction analysis developed in Ref. 2. The interfacial potential introduces further complications to this method. The total defect density and the mean depth of defects can no longer be extracted unambiguously.[2]

III. EXTENDED DIFFUSION MODEL FOR LAYERED STRUCTURES

Despite the fact that a thermal positron is a quantum-mechanical particle, its motion inside a crystal can be described with a simple diffusion model within a broad range of experimental conditions.[35] The diffusion description is valid if (i) the energy distribution of the positrons obeys Maxwell-Boltzmann statistics, (ii) the scattering events which limit the motion are approximately elastic and isotropic, and (iii) the distance scales are significantly longer than the mean free path for scattering λ.

The first two conditions are normally fulfilled because the positron motion near thermal energies inside a crystalline material is governed by scattering from acoustic phonons, at least down to 10 K.[42] Experimentally only one positron exists within the sample at any given time. The mean free path for positron-phonon scattering at room temperature is of the order of 10 Å, from which it can be concluded that the third condition is also normally fulfilled in annealed and pure single-crystal samples. An exceptional situation arises when there are boundaries inside the crystal, such as the bilayered structures presently being considered.

The information depth in positron-beam experiments is adjusted by changing the incident positron energy. Penetration depth is mostly determined at early stages of the slowing-down process.[43] The depth distribution of keV range positrons is described with an implantation profile $p(x,E)$, which serves as a source term when the stationary diffusion model is used. The implantation profile is taken[43,44] to be

$$p(x,E)=-\frac{d}{dx}\left\{\exp\left[-\left[\frac{x-\delta_i}{x_{0i}}\right]^m\right]\right\}\ , \tag{2}$$

where

$$\bar{x}=x_{0i}\Gamma\left[1+\frac{1}{m}\right]=\frac{\alpha}{\rho_i}E^n \tag{3}$$

is the mean range of positrons at energy E. The parameter δ_i in each layer is determined from the condition that the positron transmission $T(d,E)=[1-\int_0^d p(x,E)dx]$ must be continuous at all values of d measured from the surface ($d=0$).[44] ρ is the mass density of the material, $m=2.0$ is the shape parameter of the implantation profile, and both $n\approx 1.6$ and $\alpha\approx 4$ μg/cm^2 are penetration parameters of the positron.

The diffusion-annihilation equation can be written

$$D_+\frac{d^2n(x,E)}{dx}-\frac{d}{dx}[v_d(x)n(x,E)] -\lambda_{\mathrm{eff}}(x)n(x,E)+p(x,E)=0\ , \tag{4}$$

where $n(x,E)$ is the stationary positron density. D_+ denotes the positron diffusion coefficient, and $v_d(x)$ is the electric-field-dependent drift velocity. The effective annihilation rate $\lambda_{\mathrm{eff}}(x)$ gives the rate that a freely diffusing positron state disappears in the crystal, and it can be written

$$\lambda_{\mathrm{eff}}(x)=\lambda_{\mathrm{bulk}}(x)+\kappa(x)\ , \tag{5}$$

where $\lambda_{\mathrm{bulk}}(x)$ is the annihilation rate from the freely diffusing Bloch-like state, and $\kappa(x)$ is the trapping rate into the lattice defects. Trapping rate $\kappa(x)$ is directly proportional to the defect concentration, i.e., $c(x)=\kappa(x)/\mu_0$. The specific trapping rate μ_0 is characteristic to each material and each type of defect. For monovacancies μ_0 is typically of the order 10^{15} 1/s, and for dislocations 1 cm^2/s. In this work electric fields are excluded because of their effective screening in metals. In general defect profiling applications, Eq. (4) is solved numerically by reducing it to two first-order equations. In the defect-free case [$\kappa(x)=0$] there are analytical solutions, which are discussed in the Appendix.

At the interface between two different materials, positrons experience an electrostatic potential. Due to the fact that the Fermi level must be the same everywhere in the solid, there is a potential step equal to the difference in the electron chemical potentials ($\Delta\mu_-$). This contribution to the potential barrier is called the interfacial dipole, and is the same for both electrons and positrons, but the sign is opposite. The situation is analogous to the surface dipole.[45,46] The potential height for a positron is further modified by the difference of the positron chemical potentials μ_+ between the materials. In the following we will consider the interface between two metals. The potential ΔE_+ experienced by a positron at the interface between metals A and B can thus be written in the form

$$\Delta E_+ = \Delta\chi_+ = \chi_+^B - \chi_+^A = (\mu_+^B - \mu_+^A) + (\mu_-^B - \mu_-^A) , \quad (6)$$

where χ_+ is the positron affinity (values for different metals are tabulated in Ref. 47) defined as

$$\chi_+ \equiv \mu_- + \mu_+ . \quad (7)$$

We note that χ_+ is a purely bulk property, independent, e.g., on the crystallographic orientation of the interface. The more negative the value of the positron affinity is, the more preferably the positron goes into that material. In the case of an abrupt junction between two metals, ΔE_+ can be regarded as a step potential due to the short-range screening.

The interfacial potential drastically affects the motion of a thermal positron. The height of the potential is typically ~ 1 eV, whereas the thermal energy of the positron is about 2 orders of magnitude smaller. Thus, when the positron comes from a material with a more negative positron affinity, it is highly probable that it is reflected back, and *vice versa*. This can be included to the diffusion model through boundary conditions which describe the positron current through the interface.

Positron current $J(x)$ is the physical quantity, which connects the materials with each other in the diffusion picture. The current must be continuous over the interface, assuming no traps for positrons at the interface area. If we consider an interface between materials A and B at depth $x = d$ with an external surface at $x = 0$, the continuity condition leads to the boundary condition

$$D_+^A \frac{dn(x,E)}{dx}\bigg|_{x\to d^-} = D_+^B \frac{dn(x,E)}{dx}\bigg|_{x\to d^+} . \quad (8)$$

The direction of the net positron current $J(d)$ is determined by the interfacial potential ΔE_+. Between copper and silver the height ΔE_+ is theoretically 0.55 eV.[47] No experimental values of the potential difference exist. In this case, positrons prefer silver, which has been verified experimentally.[7,19] If silver is grown on copper, a thermal positron transition from the overlayer to the substrate is highly improbable (transition rate $\nu_T \to 0$), and the opposite transition rate from the substrate to overlayer then tends towards infinity ($\nu_T \to \infty$). This yields an enhanced positron current coming back to the surface (for details see Appendix). In this forward positron diode case, the backdiffusion probability has two contributions. The first term arises from the positrons implanted on the overlayer, and the second from those implanted on the substrate, transmitting through the interface and diffusing to the surface. When copper is grown on silver a reverse positron diode is formed. Transition from the substrate to the overlayer is forbidden ($\nu_T \to 0$) and the transition to the other direction is highly probable ($\nu_T \to \infty$). Backdiffusion is possible only for positrons implanted into the overlayer, and the backdiffusion probability is reduced compared to the semi-infinite case ($d = 0$).

So far, in a quantitative analysis the surface has always been treated as a totally absorbing boundary (i.e., $\nu_T \to \infty$). In our recent study it has been shown that reflection from the surface potential has a considerable effect, especially at low temperatures.[41] We will discuss later the influence of finite transition rates at the interface to numerical results. In analytical solutions, both surface and interface have been regarded as either totally absorbing or totally reflecting, due to simplicity and the ease of getting functional dependences clearer (see Appendix).

In defect profiling the profiles are usually deduced for each set of experimental data by guessing the appropriate trapping distribution $\kappa(x)$ and solving Eq. (4). The calculated backdiffusion probability is compared to the measured data. This is repeated until satisfactory agreement between the model and the experimental data is achieved. In this work we have adopted a slightly different technique. A unique defect distribution is constructed stepwise using the results obtained from the thinner structures as a base profile. The thinnest structures are analyzed first with a uniform defect profile distributed in the whole overlayer. This distribution is used as a seed for the next thinnest structure, and a new analysis is performed to study the defects in the layer extending beyond the previous one. The obtained two-piece profile is again combined with the data from the next thinnest structure in the same way. This procedure is repeated until the defect distribution of the thickest structure is analyzed. In this way we obtain an estimate for the trapping-rate distribution $\kappa(x)$ within the overlayer.

The results of the fits assuming a uniform trapping profile throughout the whole overlayer are given in Table I. Also Gaussian defect profiles were tested, but it was found that very detailed information from a single heterostructure cannot be deduced. This is mostly due to uncertainties caused by nonthermal positrons[39] returning to the surface and contributing to the measured signal. By combining the results from structures with different thicknesses we have achieved an overall picture of defect distribution in the overlayer. Different material and positron parameters for Ag and Cu used in the fitting are tabulated in Table II.

IV. RESULTS

A. "As grown" structures

In Fig. 2(a) the backdiffusion probabilities $J(E)$ measured from Cu/Ag(111) samples 1, 3, and 4 are shown. Corresponding data from a clean Cu(111) surface is also

TABLE II. Material and positron parameters for Cu and Ag used in the fitting. Relative changes to $\Delta\kappa_0$ in the positron trapping rate are given for different parameters when they are changed ±10% from the nominal value. The values correspond to those obtained from samples 3 and 10.

	Ag	Cu
Density ρ (g/cm^3)[a]	10.5	8.96
Diffusion coefficient D_+ (cm^2/s)[b]	0.9	1.7
Positron lifetime τ (ps)[c]	128	110
α (μg/cm^2)[d]	4.0	4.0
m[d]	2.0	2.0
n[d]	1.6	1.6
Specific trapping rate μ_0		
to vacancies (10^{15} s^{-1})	1.0[e]	0.8[e]
to dislocations (cm^2/s)	1.8	1.5[f]
	Sample 3	Sample 10
$\Delta\kappa_0/\kappa_0$ due to δD_+	−0.10	−0.25
$\Delta\kappa_0/\kappa_0$ due to $\delta\alpha$	0.30	0.15
$\Delta\kappa_0/\kappa_0$ due to δm	0.14	0.05
$\Delta\kappa_0/\kappa_0$ due to δn	−0.55	−0.50

[a]Reference 52.
[b]Reference 40.
[c]Reference 33.
[d]Reference 43.
[e]Reference 48.
[f]Reference 49.

presented for comparison. The diffusion length L_+ for positrons, in copper at room temperature is $L_+ = 1300 \pm 50$ Å (Ref. 41) and in Ag $L_+ = 1100 \pm 100$ Å.[40] During the preparation of the thinnest layer, the growth rate was 6.5 Å/min, while the thicker ones were grown with the rate 11.2 Å/min. We observe that the backdiffusion probability is increased as the layers become thicker. In sample 1 a significant part of the positrons is implanted into the substrate in the used energy range. Due to the reflecting positron potential at the interface they have no possibility of returning to the entrance surface. This phenomenon is even more drastic at lower coverages, where implantation on the layer can be almost totally neglected.[19] Backdiffusion probability is also reduced by those positrons implanted into the overlayer but escaping to the substrate. Furthermore, backdiffusion is affected by defects capable of trapping positrons. Another specific feature in $f_+(E)$ curves is that even from the 2800-Å-thick Cu layer, $f_+(0)$ values are reduced from those obtained from a defect-free Cu(111) (see Table I). This indicates that surface branching is different from that at the Cu(111) surface, which can be interpreted to be due to the disordered surface region.

When Ag/Cu(111) structures are investigated, changes in the measured $J(E)$ curves are not so obvious. In Fig. 2(b) we show the $J(E)$ data measured from Ag/Cu(111)—samples 8 and 12—and the corresponding curve for bulk Ag(111). The growth rate has been 13.8 Å/min. In the case of the forward positron potential, the backdiffusion probability should increase from a semi-infinite crystal due to a reverse interfacial potential for positrons implanted into the overlayer (see Appendix). This kind of enhancement is not observed, which is attributed to positron trapping to vacancy-type defects in the Ag overlayer.

From the profiling it was observed that positron traps are confined to the near-interfacial region. The average defect density decreases with layer thickness, and thus in this study we are able only to follow this reduction of de-

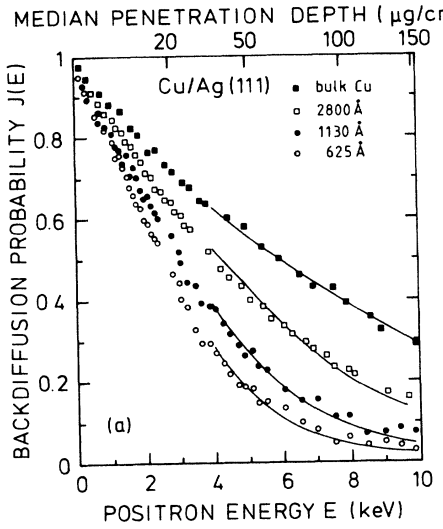

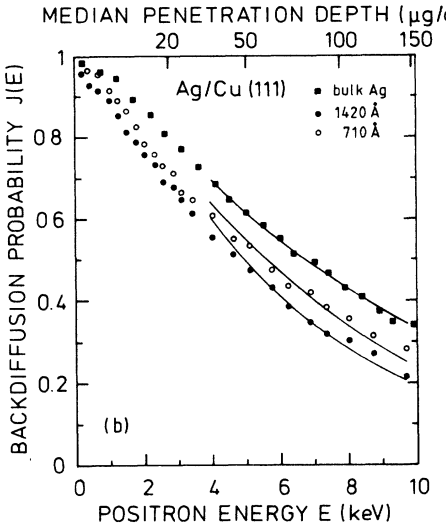

FIG. 2. (a) Experimental backdiffusion probabilities J as a function of the incident beam energy E from Cu/Ag(111) structures: from a clean defect-free Cu sample; 2800-Å-thick Cu/Ag(111); 1130-Å-thick Cu/Ag(111); and 625-Å-thick Cu/Ag(111). Curves are normalized by direct extrapolation to the experimental yields at zero energy. Solid lines correspond to the fits to the diffusion model with a uniform defect distribution. (b) Experimental backdiffusion probabilities J as a function of the incident positron energy E from Ag/Cu(111) structures: a clean defect free Ag sample; 710-Å-thick Ag/Cu(111); and 1420-Å-thick Ag/Cu(111). Curves are normalized by direct extrapolation to the experimental yields at zero energy. Solid lines correspond to the least-squares fits to the diffusion model with a uniform defect distribution.

fects. The energy interval included in the diffusion fit has been limited to 4 keV $\leq E_{inc} \leq$ 10 keV. The lower limit is set by epithermal effects, which can be seen as sharpening of $f_+(E)$ curve at low incident energies.[39,40]

In the Cu/Ag(111) structures the positron density is very low in the overlayer near the interface. All positrons from this region tend to diffuse to the substrate. This causes the trapping information to be originated mainly from the near-surface area. Additionally, this feature appears to make the Cu/Ag(111) system more sensitive to different systematic error sources in the analysis than the opposite system (see Sec. IV C). Trapping rate values κ_0 corresponding to uniform defect distribution throughout the overlayer are given in Table I. The defect density is a slowly varying function of overlayer thickness (see Sec. V A). Hence, uniform defect distributions give us relatively accurate average densities, making it possible for easy mutual comparison between growths. Sensitivity to the near-interface defects was tested by using a uniform defect profile and introducing a defect-free region outwards from the interface. We noticed that one could add a defect-free region roughly $\approx$30% of the total overlayer thickness without seeing more than a 10% change in the fitted κ_0. On the other hand, at the opposite system, Ag/Cu(111), positron density is enhanced near the interface, and the detection efficiency for defects is increased. In this system a defect-free region of only a few tens of angstroms in thickness is needed to drastically change the values of κ_0. From this we conclude that the ability to observe defects with the low-energy positron-beam technique depends on the relative positron energy levels in the studied system.

B. Effect of growth conditions

Tailoring the layered structures for different purposes demands a precise knowledge on the effect of the growth parameters to the resulting heterostructure. In UHV evaporations (MBE growth) several factors affect the final result. The growth rate is determined mainly by adjusting the material flux via the oven temperature. Conditions of the substrate influence most the crystal quality. Interactions between substances present during the growth, mobility of the adatoms on the surface, and characteristics of the substrate are the physical phenomena associated to the quality. They can be controlled by adjusting the substrate temperature, by choice of materials, and by proper pre-evaporation treatment of the substrate. Post-evaporation heat treatment can make the layer better, but there is always the danger of intermixing of the materials. In this part of the work we have not made any systematic study of these factors, but we will just demonstrate the ability of positrons to detect structural changes in the layers.

The effect of the substrate temperature was studied by growing two 1175-Å-thick Ag/Cu(111) structures (samples 10 and 11). In the first growth the substrate was held at room temperature, whereas the latter structure was made at 100 °C. Higher substrate temperatures were not studied because of Cu/Ag mixing at elevated temperatures.[29] The $J(E)$ data from these structures are presented in Fig. 3. The increase in the positron diffusion length at higher-temperature growth is directly observed. This indicates a reduced defect density. Assuming uniform defect profiles we get trapping rates $\kappa_0 = 2.0 \times 10^{10}$ s^{-1} and $\kappa_0 = 1.1 \times 10^{10}$ s^{-1} for the two cases, respectively. The defect density is reduced by a factor of 2. The higher substrate temperature increases the mobility of atoms at the surface, and it is more likely for the adatom to find a more suitable site for growth and to fill a vacant lattice site more efficiently.

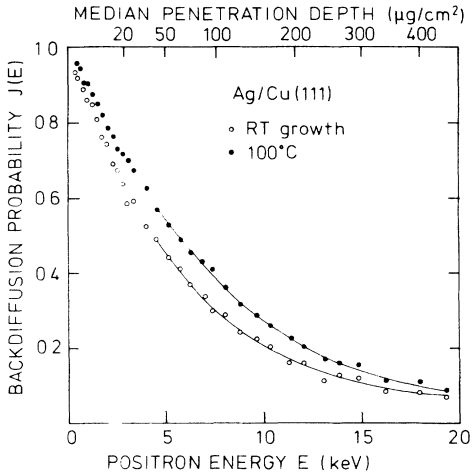

FIG. 3. Measured backdiffusion probabilities $J(E)$ from a 1175-Å Ag/Cu(111) structure grown on the substrate at room temperature, and a 1175-Å Ag/Cu(111) structure grown on the substrate at 100 °C.

No direct test on the growth-rate dependence to the defect density was done. But by comparing 625- and 800-Å-thick Cu/Ag(111) structures grown with rates 6.5 and 11.2 Å/min, respectively, a reduction of 20% in the trapping rate for the slower growth rate can be observed (see Table I). This effect is so minor that it cannot be directly attributed to a change in the growth rate. Secondary effects, such as differences in substrate preparation, may also be a reason for this observation.

A low-temperature heat treatment (5 min at 200 °C) was given to all Cu/Ag(111) structures except the 2800-Å-thick structures (samples 1–3). Also thinner layers (from 10 Å up to 200 Å) were studied, and AES measurements showed that this low-temperature heating caused Ag enrichment to the surface. This is in agreement with observations of Gibson and Dobson[27] and Shapiro *et al.*[26] Other phenomena observed in these thinner structures will be published separately.[19] In Figs. 4(a) and 4(b) the $J(E)$ curves are shown from "as grown" and annealed 65- and 1135-Å-thick Cu/Ag(111) structures, respectively.

C. Systematic error sources

In the diffusion-model analysis, several uncertainties exist that affect the results. The most important of them is caused by errors in the layer-thickness determination. Uncertainties in the evaluation of the backdiffusion probability are caused by the effect of epithermal positrons. The knowledge of different positron parameters describ-

ing their interactions with solids is still limited, even though data are rapidly improving.[44,40] The values of the parameters used are listed in Table II. When the effects of these factors are estimated, we consider the measurements from the 1175-Å-thick Ag/Cu(111) structure (sample 10) and from the 1135-Å-thick Cu/Ag(111) structure (sample 3).

The error in thickness determination is estimated to be ±20%. This is the main error source in the extracted κ_0 values. At the limits of ±20% from the nominal layer thickness, the trapping rate κ_0 varies in sample 3 from 8.3×10^{10} to 1.2×10^{11} s^{-1} ($-25\% \le \Delta\kappa_0/\kappa_0 \le 10\%$) and in sample 10 from 1.7×10^{10} to 2.6×10^{10} s^{-1} ($-15\% \le \Delta\kappa_0/\kappa_0 \le 30\%$).

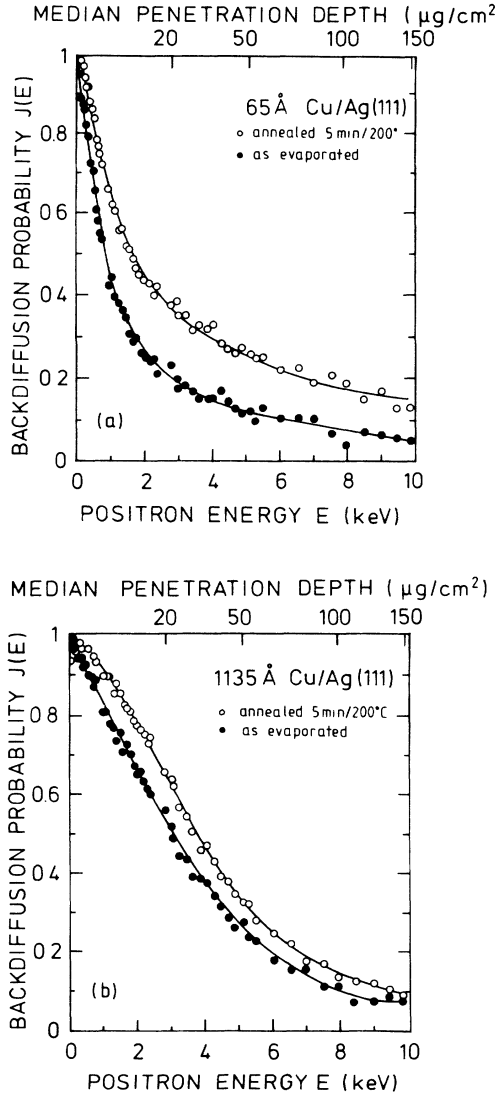

FIG. 4. (a) Backdiffusion probability $J(E)$ from a 65-Å-thick Cu/Ag(111) structure measured as grown and after heat treatment of 5 min at 200 °C. The solid lines are a guide for the eye only. (b) Backdiffusion probability $J(E)$ from a 1135-Å-thick Cu/Ag(111) structure measured as grown and after heat treatment of 5 min at 200 °C. The solid lines are a guide for the eye only.

Another important source of systematic errors is connected to the evaluation of the backdiffusion probability. Positrons escaping from the crystal prior to complete thermalization (i.e., epithermal positrons) give a different signal than the thermal ones. As discussed before, the direct extrapolation of $f_+(0)$ from the measured curve leads to an overestimation of the trapping rate κ_0, because the actual $f_+(0)$ due to thermal positrons is smaller than the measured one.[39] While the trapping probability for the epithermal positrons is energy dependent, it is difficult to obtain quantitative information at lower incident energies, where the fraction of epithermal positrons is considerable. In this work we included only the energy interval 4 keV $\le E_{inc} \le$ 10 keV for the analysis of defect profiles. Above 4 keV the signal is mostly from thermal positrons.[39,40]

Parameters describing the positron implantation and positron motion in solids also scale the trapping rates. We studied the effect of uncertainties in the penetration parameters α and n [Eq. (3)], the shape parameter m [Eq. (2)], and the diffusion coefficient D_+ [Eq. (4)]. We found that the trapping rate depends linearly on these quantities. Relative changes are given in Table II for both systems. We note that the trapping rate is more sensitive to errors in the Cu/Ag(111) system than those in Ag/Cu(111). The method is most sensitive for errors in the values of n. Regardless, it must be remembered that converting the trapping rates to defect densities includes the specific trapping-rate characteristic for each type of defect. These factors also have large uncertainties, which are approximately ±50%. The defects can thus be more accurately compared on a relative scale between different structures.

V. DISCUSSION

A. Defect profiles

Positrons are sensitive to open volume defects. In each type of defect, positrons have different annihilation characteristics. In this work, the positron current diffusing back to the surface is used for defect characterization. The measured signal is therefore not sensitive to the type of the defects, only to their depth-dependent concentration. Matching two different materials with different lattice constants and structures breaks the translational symmetry of the crystal. This misfit causes elastic strain near the interface which is accommodated by creating misfit dislocations. We discuss positron trapping in Ag/Cu(111) structures, assuming that it is due to either monovacancies or misfit dislocations. The present data cannot be used to distinguish between the two possibilities.

In the previous section we introduced the trapping rates $\kappa(x)$ obtained by using the diffusion model. The trapping rate is directly proportional to the defect concentration, i.e., $c(x)=\kappa(x)/\mu_0$. For vacancies in Cu we have used the value $\mu_0^{Cu}=8\times10^{14}$ s^{-1} (Ref. 48) and in Ag $\mu_0^{Ag}=1\times10^{15}$ s^{-1} (Ref. 48). In copper, the specific trapping rate for dislocations is found to be $\mu_0^{disl,Cu}=1.5$ cm^2/s (Ref. 49). We have utilized the value $\mu_0^{disl,Ag}=1.8$

cm^2/s also for dislocations in silver due to lack of experimental data. It has also been reported that positrons have a different specific trapping rate for screw and edge dislocations in iron.[50] The differences in any case are minor when compared to the general uncertainty. Consequently, we have adopted a single value describing positron trapping to dislocations. The accuracy of the specific trapping rate is about ±50%, which makes them the primary source of uncertainty in the absolute defect concentrations.

In Fig. 5 the stepwise constructed defect profiles $c(x)$ are shown. In both systems the thinnest structure was analyzed first. The results are given both in terms of vacancy concentration (cm^{-3}) and dislocation density (cm^{-2}). When the total defect concentration (i.e., the area of the defect profile) is analyzed, we observe only a slight increase in the total defect density as a function of thickness. This indicates also that defects are confined within the vicinity of the interface in both studied systems. This is very understandable, because most of the misfit is accommodated near the interface region ($d < 100$ Å). Unfortunately, the present technique does not allow us to study such thin structures in more detail.

In the defect profile of the Cu/Ag(111) structure, only three layers (samples 2–4) are included. Sample 1, grown with a different rate, has been omitted from the analysis. We extract a single profile based on the successive analysis, and the result is given as a solid line in Fig. 5. In the analysis of the Ag/Cu(111) structure, we have used seven (samples 5–10, 12) different samples. The scattering of the results obtained from different layers does not allow us to extract a unique profile. In Fig. 5 the upper and lower limits are given for the profile. The upper limit was constructed using data measured from samples 2, 5, and 6, and the lower limit correspondingly from samples 1, 4, and 7. The true profile lies in the shaded area. As discussed above, it is impossible to get information from the near-interface region with the present technique on the Cu/Ag(111) structure, and, therefore, the profile has been terminated 200 Å from the interface. However, it is also possible to observe defects near interface in the retarding positron potential case by following the evolvement of the substrate signal in the Doppler broadening measurements. In that case one is actually following the positron current over the interface.

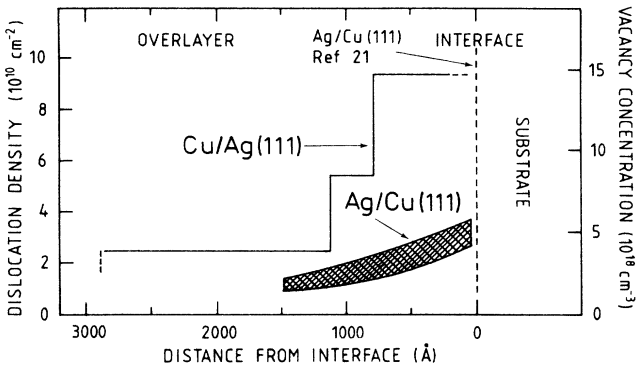

FIG. 5. Extracted defect profiles $c(x)$ constructed by iterative profiling. $c(x)$ is given both in terms of dislocation density and vacancy concentration. The profile of the Cu/Ag(111) structure is extracted from data measured from samples 2–4. The upper limit of the Ag/Cu(111) defect profile is achieved by analyzing samples 2, 5, and 6, and the lower limit by analyzing samples 1, 4, and 7. The true profile lies within the shaded area. The arrow indicates the dislocation density observed in Ref. 21 at layer thicknesses 1–20 Å.

The profiles shown in Fig. 5 describe the reduction of the defect density within the layer. If the dislocation picture is adopted, it occurs as a gradual termination of dislocations that have a component directed normal to the sample surface. If an exponential law $c(x) = c_0 \exp(-d/d_0)$ is applied to measured data, the characteristic attenuation lengths of dislocations d_0 have a value of 1500 Å in the Cu/Ag(111) system and 1200 Å in Ag/Cu(111).

In the Ag/Cu(111) system (i.e., the forward positron potential case) we do not observe an enhancement suggested by the diffusion model (see Sec. III and Appendix). In order to verify this a small lattice-mismatch system, e.g., Cu grown on a Ni substrate, should be investigated. The defect contribution to the positron motion is then expected to be smaller. The excess energy that positrons gain at the interface in this system must also be considered, because parameters such as the mean free path for different scattering events, and the specific trapping rate, describing positron interaction with the solid, are strongly energy dependent. As a first approximation, when other uncertainties are large, the presented diffusion model is appropriate. But if detailed information is desired, an alternative approach to describe the rethermalization is needed. For example, a transport approach developed to model hot-positron attenuation in layered structures by Huttunen *et al.*[31] and to describe epithermal positrons by Kong and Lynn[51] would be helpful. Also, Monte Carlo simulation of these processes would be straightforward. Further experimental and theoretical work is required in order to clarify the importance of these effects.

B. Comparison between systems

When copper is grown on the Ag(111) surface, more defects capable of positron trapping are observed than in the opposite structure. A factor from 3 to 5 difference in the defect concentration between the two systems is observed, depending on the layer thickness. This behavior is already predicted at early stages of crystal growth. Both systems grow with the Stranski-Krastanov mode, but in the Cu/Ag(111) system only 1 monolayer is formed before island formation starts, whereas with silver grown on Cu(111) at least 3 monolayers are completed.[19] Lattice constants for copper and silver are 3.61 and 4.09 Å,[52] respectively. While the crystal growth begins coherently with the substrate, the first copper layer is more open than bulk copper. This benefits the creation open-volume defects which attract positrons. In the opposite case, Ag atoms effectively fill the Cu(111) surface, resulting in compression-type disorder. These defects cannot be observed for positrons.

Dislocation structures at thin (1–20 Å) layers have been studied by electron diffraction (RHEED, TED) and electron microscopy (TEM), both in Cu/Ag(111) (Ref. 53) and Ag/Cu(111) structures.[21] In the previous systems only few isolated sections of interface which contain misfit dislocations were found. In the Ag/Cu(111) structure, Vook and Horng were able to identify three different types of dislocations, two of which were confined parallel to the interface. They accommodate misfit very effectively. One of the dislocation types has a component along the interface normal. When their results are combined, the reported dislocation density is of the order of 10^{11} cm^{-2}. This confirms well our experimental results at the low layer thickness limit. For the 475-Å-thick structure we obtain a dislocation density 3×10^{10} cm^{-2}, assuming a uniform distribution of defects. The recent observations of Tyliszczak *et al.*[17] also suggest that disorder is mostly limited to the near-interface area. According to their surface extended energy-loss fine-structure (SEELFS) measurements, 5 monolayers of Cu on Ag(111) is enough to produce a layer that grows with the lattice constant of copper.

C. Finite transition rates

So far, all the results given in this paper have been obtained by assuming either total transmission or reflection of the positron from the surface or from the interfacial potential. As fully quantum-mechanical particles, positrons have a finite transition rate in the vicinity of potential differences, as has recently been demonstrated at a Cu(111) surface.[41] In the present work we have assumed that the surface is totally absorbing, which gives an upper limit to defect concentrations. The finite transition rates at the interface have been studied in the samples 3 and 10.

The transition rate through an interfacial potential ν_T can easily be calculated for a thermal positron. We adopted a potential step model with a plane-wave description for positrons and a theoretical value for the potential difference $\Delta\chi_+=0.55$ eV.[47] When incorporated into the diffusion model, this approach leads to a transition rate ν_T as a function of layer thickness and diffusion length.

In Cu/Ag(111) structures a finite transition rate at the interface reduces the transport from the overlayer to the substrate, as the reflection probability is enhanced. A test was done with the data measured from the 1134-Å-thick Cu layer. Theoretically, the transition rate can be estimated to be $\nu_T\approx5\times10^3$ m/s. Using this value with a simple uniform defect distribution model gives $\kappa_0=1.2\times10^{11}$ s^{-1}, whereas for a totally absorbing interface ($\nu_T\rightarrow\infty$), a value $\kappa_0=1.1\times10^{11}$ s^{-1} is obtained. At the opposite structures [Ag/Cu(111)], the backdiffusion probability $J(E)$ has two contributions: those implanted on the overlayer and those on the substrate. The former ones thermalize at the overlayer and are not able to overcome the potential step at the interface. The latter contribution becomes dominant for the thin layers. The influence of changes in the latter part of the positron flux was tested with the data from 1175-Å-thick Ag/Cu(111) structure. The values for κ_0 1.6×10^{10} s$^{-1}\leq\kappa_0\leq2.0\times10^{10}$ s^{-1} were obtained for totally reflecting and absorbing interfaces, respectively. From these values it can be concluded that the reflection has no major effect when analyzing thick structures. Nevertheless, it must be considered when studying thinner overlayers.

D. Intermixing versus defects

Intermixing is a phenomenon present to some extent at most interfaces. For example, the studied Cu/Ag system is exceptional among the noble metals in the sense of having a positive heat of formation, and thus forming a sharp and stable interface at room temperature.[54] At elevated temperatures, also Cu and Ag readily mix. The alloy formation causes broadening of the interfacial potential, which limits the use of the presented diffusion model. In this work we studied the effect of a 5-min heat treatment at 200 °C to Cu/Ag(111) structures. When these measurements were compared to those from the as-evaporated samples, we observed a clear change, which can be attributed partly to the broadening effect and partly to the recovery of defects. These phenomena are difficult to distinguish and we are not able to satisfactorily separate them with the present technique.

From Figs. 4(a) and 4(b) it can be directly seen that we observe an enhanced backdiffusion that can be connected to the annealing treatment. When the interfacial potential is assumed abrupt and all enhancement is attributed to the recovery of the defects, diffusion model analysis can be applied. This analysis was performed to the $J(E)$ curves measured from the samples 1–3 after annealing at 200 °C for 5 min. With uniform defect distribution fits, it was observed that defect density is reduced by the factor of approximately 2.5. The values for κ_0 are listed in Table I. The description of the data is not very good (reduced χ^2 values ~3.0).

Another approach is to explain changes in $J(E)$ curves by interdiffusion. In AES experiments we observed the enrichment of Ag to the surface even with the used moderate annealing cycle at thin coverages (<100 Å), in accordance with earlier experiments.[27] Lattice and grain-boundary diffusion are the possible intermixing mechanisms for Ag and Cu, due to their small mutual solubility below 500 °C.[28] However, we cannot distinguish between these processes in the present experiments, and further studies with finer layer thickness and temperature scales associated with, e.g., depth profiling with AES, would be needed. Nevertheless, it is evident that the possibility of the alloying and its influence on positron behavior in epitaxial layers must be considered when experiments are interpreted. The diffusion-induced microstructure may change totally positron interaction with solids near the interface. Both diffusion mechanisms may explain the increased Ps yields presented in Fig. 4. Grain-boundary diffusion will open new channels for positrons to encounter the surface. On the other hand, lattice diffusion may create a uniform alloy layer, especially at the thinnest structures, lowering the interface potential, and hence increasing the positron escape from the bulk to the surface. Also, if the change in interface po-

tential becomes gradual enough, thermal positrons may overcome the potential even if it is repulsive.

VI. CONCLUSIONS

We are reporting what we believe to be the first quantitative studies of defect distributions in layered heteroepitaxial structures with monoenergetic positrons. We have applied the *nondestructive* positron technique to epitaxial Cu/Ag(111) and Ag/Cu(111) structures within the overlayer thickness varying from 250 up to 2800 Å. Our main results are as follows.

(1) The positron diffusion model has been extended to the layered structures.

(2) We are able to apply the extended model to the data measured from the Cu/Ag(111) and Ag/Cu(111) structures, and to determine the defect distribution in them. The defect densities are typically of the order 10^{10} cm^{-2}, assuming the defects to be dislocations, or, alternatively, 10^{18} cm^{-3} for the vacancies.

(3) Defects are found to be confined near the interface. Assuming a exponential reduction as the overlayer grows, characteristic attenuation lengths of 1500 Å in Cu/Ag(111) and 1200 Å in Ag/Cu(111) for the defect densities are found.

(4) In the Cu/Ag(111) system we observe more defects with positrons than in the Ag/Cu(111) system. This can be attributed to the lattice constants. When copper is grown on Ag(111) ($a_{Cu} < a_{Ag}$), it is more likely that open-volume defects are created than in the opposite system.

(5) The observed defect densities in the thin-film limit are consistent with earlier observations obtained with electron microscopy.

(6) We have also demonstrated the influence of growth parameters on layer quality and the ability of positrons to observe them.

(7) We will discuss the results of our annealing experiments in terms of structural changes in the overlayer induced either by recovery of defects or by interdiffusion at the interface.

ACKNOWLEDGMENTS

We thank R. M. Nieminen, M. Puska and P. J. Schultz for useful discussions. One of us (P.A.H.) is grateful to Emil Aaltonen Foundation for financial support. Work performed at Helsinki University of Technology was supported by the Academy of Finland.

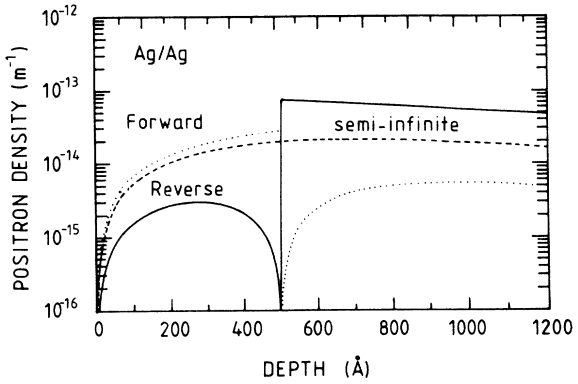

FIG. 6. Positron densities for a 500-Å-thick Ag/Ag structure with different boundary conditions when the incident positron energy is 5 keV. The solid line corresponds to the reverse positron diode, the dotted line to the forward positron diode, and the dashed line to the semi-infinite crystal.

APPENDIX: POSITRON DIFFUSION IN DEFECT-FREE BILAYERED STRUCTURE

In order to get a clear picture of positron motion in the presence of a material interface, we consider a defect-free bilayered structure, and apply the diffusion model to it. In numerical calculations the material has been assumed to be silver at both sides of the interface. If the positron affinity of the layer material is smaller than that corresponding to the substrate, a potential step prevents the escape of positrons implanted on the substrate. This can be regarded as a reverse positron diode, and the backdiffusion probability at the surface is drastically reduced. A forward positron diode is formed when the substrate has a larger positron affinity than the overlayer. In this case, positrons achieve additional energy from the interface, and the backdiffusion probability is increased.

For a reverse positron diode, all positrons approaching the interfacial area end up into the substrate. Appropriate boundary conditions describing this process are

$$n(x \to d^-) = 0 \ , \qquad D_o^+ \left.\frac{dn}{dx}\right|_{x \to d^-} = D_s^+ \left.\frac{dn}{dx}\right|_{x \to d^+} \ , \tag{A1}$$

where D_o^+ and D_s^+ correspond the positron diffusion coefficient for a positron in the overlayer and in the substrate, respectively. This case is identical to the positrons returning back to the entrance surface in thin films.[55]

By solving the diffusion equation with Green's-function technique, we get for the positron density in the overlayer

$$n(x<d) = \frac{L_+^o}{D_o^+ \sinh(d/L_+^o)} \left[\sinh[(d-x)/L_+^o] \int_0^x \sinh(t/L_+^o) p(t) dt + \sinh(x/L_+^o) \int_x^d \sinh[(d-t)/L_+^o] p(t) dt \right] , \tag{A2}$$

and in the substrate

$$n(x>d)=\frac{L_+^s\exp(d/L_+^s)}{D_s^+}\left[\exp(-x/L_+^s)\int_d^x\cosh[(d-t)/L_+^s]p(t)dt+\cosh[(d-x)/L_+^s]\int_x^\infty\exp(-t/L_+^s)p(t)dt\right]$$
$$+\frac{L_+^s\exp(d/L_+^s)}{D_s^+\sinh(x/L_+^o)}\exp(-x/L_+^s)\int_0^d\sinh(t/L_+^o)p(t)dt\ . \tag{A3}$$

These solutions are given in Fig. 6 for a 500-Å-thick Ag/Ag structure with a solid line. The positron incident energy is assumed to be 5 keV. The solution for a normal semi-infinite case is shown for comparison with a dashed line. It is observed that the positron density for a reverse positron diode is extremely low at the near-interface area. This demonstrates that direct information on defects in this region cannot be obtained. It is possible to get this data indirectly by following the fraction of positrons annihilating at the substrate with a Doppler-broadening technique.

Return to the entrance surface is possible only for those positrons implanted on the overlayer. This reduces remarkably the backdiffusion probability (Fig. 7, solid line). For a reverse positron diode the backdiffusion probability can be deduced from Eqs. (5) and (A2) to be

$$J_d(E)=\frac{1}{\sinh(d/L_+^o)}\int_0^d\sinh[(d-t)/L_+^o]p(t)dt\ . \tag{A4}$$

The difference between the two positron diodes is described by the boundary conditions, which for the reverse positron diode are given in Eq. (A1). For a forwarding case the boundary conditions become

$$n(x\to d^+)=0\ ,$$
$$D_o^+\left.\frac{dn}{dx}\right|_{x\to d^-}=D_s^+\left.\frac{dn}{dx}\right|_{x\to d^+}\ . \tag{A5}$$

Again we can express the positron densities for a defect free crystal in the overlayer as

$$n(x<d)=\frac{L_+^o}{D_o^+\cosh(d/L_+^o)}\left[\cosh[(d-x)/L_+^o]\int_0^x\sinh(t/L_+^o)p(t)dt+\sinh(x/L_+^o)\int_x^d\cosh[(d-t)/L_+^o]p(t)dt\right]$$
$$+\frac{L_+^o\exp(d/L_+^s)}{D_o^+\cosh(d/L_+^o)}\sinh(x/L_+^o)\int_d^\infty\exp(-t/L_+^s)p(t)dt\ , \tag{A6}$$

and in the substrate as

$$n(x>d)=\frac{L_s^+\exp(d/L_+^s)}{D_s^+}\left[\exp(-x/L_+^s)\int_d^x\sinh[(t-d)/L_+^s]p(t)dt+\sinh[(x-d)/L_+^s]\int_x^\infty\exp(-t/L_+^s)p(t)dt\right]\ , \tag{A7}$$

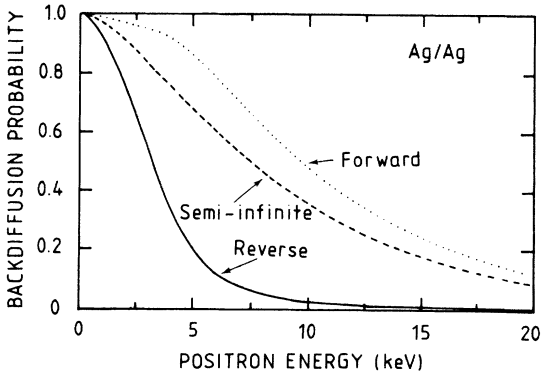

FIG. 7. Backdiffusion probabilities for a 500-Å-thick Ag/Ag structure as a function of incident positron energy. The solid line corresponds to the reverse positron diode, the dotted line to the forward positron diode, and the dashed line to the semi-infinite crystal.

which are shown in Fig. 6 with the dotted line.

The backdiffusion probability consists of two different components. On the one hand, there is a component from positrons implanted on the overlayer, and their escape to the substrate is prevented by the interfacial potential. On the other hand, there is a component from hot positrons emitted from the substrate to the overlayer side. The solution for backdiffusion probability can be derived from Eqs. (5) and (A5) to be

$$J_d(E)=\frac{1}{\cosh(d/L_+^s)}\int_0^d\cosh[(d-t)/L_+^s]p(t)dt$$
$$+\exp(d/L_+^s)\int_d^\infty\exp(-t/L_+^s)p(t)dt\ , \tag{A8}$$

and it is drawn as a function of energy for a 500-Å Ag/Ag structure with a dotted line in Fig. 7. This solution has been considered in the case of a constant implantation profile by Debowska *et al.*[56]

*Present address: Outokumpu Group, P.O. Box 280, SF-00101 Helsinki 10, Finland.
[1]P. J. Schultz and K. G. Lynn, Rev. Mod. Phys. **60**, 701 (1988).
[2]J. Mäkinen, A. Vehanen, P. Hautojärvi, H. Huomo, J. Lahtinen, R. M. Nieminen, and S. Valkealahti, Surf. Sci. **175**, 385 (1986).
[3]K. G. Lynn, D. M. Chen, B. Nielsen, R. Pareja, and S. Myers, Phys. Rev. B **34**, 1449 (1986).
[4]J. Keinonen, M. Hautala, E. Rauhala, V. Karttunen, A. Kuronen, J. Räisänen, J. Lahtinen, A. Vehanen, E. Punkka, and P. Hautojärvi, Phys. Rev. B **37**, 8269 (1988).
[5]P. J. Schultz, E. Tandberg, K. G. Lynn, B. Nielsen, T. E. Jackman, M. W. Denhoff, and C. G. Aers, Phys. Rev. Lett. **61**, 187 (1988).
[6]P. J. Schultz, K. G. Lynn, W. E. Frieze, and A. Vehanen, Phys. Rev. B **27**, 6626 (1983).
[7]A. Vehanen, P. Huttunen, J. Mäkinen, and P. Hautojärvi, J. Vac. Sci. Technol. A **5**, 1142 (1987).
[8]For a review on the epitaxial growth, see, e.g., *Epitaxial Growth,* edited by J. Matthews (Academic, New York, 1975); R. Bruinsma, and A. Zangwill, J. Phys. (Paris) **47**, 2055 (1986).
[9]See, e.g., F. Fujita and M. Hirabayashi, in *Microscopic Methods in Metals,* edited by U. Gonser (Springer, Berlin, 1986).
[10]S. N. G. Chu, A. T. Macrander, K. E. Strege, and W. D. Johnston, Jr., J. Appl. Phys. **57**, 249 (1985).
[11]L. C. Feldman, J. W. Meyer, and S. T. Picraux, *Materials Analysis by Ion Channeling* (Academic, New York, 1982).
[12]D. W. Gidley, Phys. Rev. Lett. **62**, 811 (1989).
[13]E. Bauer, Z. Kristallogr. **110**, 372 (1958).
[14]C. T. Horng and R. W. Vook, J. Vac. Sci. Technol. **11**, 140 (1974).
[15]M. J. Gibson and P. J. Dobson, J. Phys. F **5**, 864 (1975).
[16]E. Bauer, Appl. Surf. Sci. **11/12**, 479 (1982).
[17]T. Tyliszczak, A. P. Hitchcock, and M. DeCrescenzi, Phys. Rev. B **38**, 5768 (1988).
[18]T. Tyliszczak, M. DeCrescenzi, and A. P. Hitchcock, Phys. Rev. B **37**, 10 664 (1988).
[19]P. A. Huttunen and A. Vehanen (unpublished).
[20]A. P. Shapiro, T. C. Hsieh, A. L. Wachs, T. Miller, and T.-C. Chiang, Phys. Rev. B **38**, 7394 (1988).
[21]R. W. Vook and C. T. Horng, Philos. Mag. **33**, 843 (1976).
[22]R. W. Vook, C. T. Horng, and J. E. Macur, J. Cryst. Growth **31**, 353 (1975).
[23]C. T. Horng and R. W. Vook, Surf. Sci. **54**, 309 (1976).
[24]Y. Namba and R. W. Vook, Thin Solid Films **82**, 165 (1981).
[25]Y. Borensztein, Europhys. Lett. **4**, 723 (1987).
[26]A. P. Shapiro, A. L. Wachs, and T.-C. Chiang, Solid State Commun. **58**, 121 (1986).
[27]M. J. Gibson and P. J. Dobson, J. Phys. F **5**, 1828 (1975).
[28]J. M. Schoen, J. M. Poate, C. J. Doherty, and C. M. Melliar-Smith, J. Appl. Phys. **50**, 6910 (1979).
[29]J. R. Pitts, A. W. Czanderna, and T. M. Thomas, J. Vac. Sci. Technol. A **4**, 1671 (1986).
[30]D. W. Gidley and W. E. Frieze, Phys. Rev. Lett. **60**, 1193 (1988).
[31]P. A. Huttunen, A. Vehanen, and R. M. Nieminen, Phys. Rev. B **40**, 11 923 (1989).
[32]J. Lahtinen, A. Vehanen, H. Huomo, J. Mäkinen, P. Huttunen, K. Rytsölä, M. Bentzon, and P. Hautojärvi, Nucl. Instrum. Methods B **17**, 73 (1986).
[33]For a general review on positrons in solids, see, e.g., *Positrons in Solids,* edited by P. Hautojärvi (Springer, Berlin, 1979); *Positron Solid-State Physics,* Proceedings of International School of Physics "Enrico Fermi," Course LXXXIII, edited by W. Brandt and A. Dupasquier (North-Holland, Amsterdam, 1983).
[34]The Cu bar was manufactured at Tampere University of Technology from Cu supplied by Outokumpu Corporation.
[35]For a review on the thermal positron motion in solids, see T. McMullen, in *Positron Annihilation,* Proceedings of the 7th International Conference on Positron Annihilation, New Delhi, 1985, edited by P. C. Jain, R. M. Singru, and K. P. Gopinathan (World Scientific, Singapore, 1985), p. 657.
[36]D. A. Fischer, K. G. Lynn, and D. W. Gidley, Phys. Rev. B **33**, 4479 (1986).
[37]O. V. Boev, M. J. Puska, and R. M. Nieminen, Phys. Rev. B **36**, 7786 (1987).
[38]R. H. Howell, I. J. Rosenberg, and M. J. Fluss, Phys. Rev. B **34**, 3069 (1986).
[39]H. Huomo, A. Vehanen, M. D. Bentzon, and P. Hautojärvi, Phys. Rev. B **35**, 8252 (1987).
[40]E. Soininen, H. Huomo, P. A. Huttunen, J. Mäkinen, A. Vehanen, and P. Hautojärvi, Phys. Rev. B (to be published); H. Huomo, E. Soininen, and A. Vehanen, Appl. Phys. A (to be published).
[41]D. T. Britton, P. A. Huttunen, J. Mäkinen, E. Soininen, and A. Vehanen, Phys. Rev. Lett. **62**, 2413 (1989).
[42]P. Kubica and A. T. Stewart, Phys. Rev. Lett. **34**, 852 (1975).
[43]S. Valkealahti and R. Nieminen, Appl. Phys. A **32**, 95 (1983); **35**, 51 (1984).
[44]A. Vehanen, K. Saarinen, P. Hautojärvi, and H. Huomo, Phys. Rev. B **35**, 4606 (1987).
[45]B. Y. Tong, Phys. Rev. B **5**, 1436 (1972).
[46]C. A. Murray, A. P. Mills, and J. E. Rowe, Surf. Sci. **100**, 647 (1980).
[47]M. Puska, P. Lanki, and R. M. Nieminen, J. Phys. Condens. Matt. **1**, 6081 (1989).
[48]H. E. Schaefer, in *Positron Annihilation,* Proceedings of the 6th International Conference on Positron Annihilation, The University of Texas at Arlington, 1982, edited by P. G. Coleman, S. C. Sharma, and L. M. Diana (North-Holland, Amsterdam, 1982), p. 369.
[49]B. T. A. McKee, S. Saimoto, A. T. Stewart, and M. J. Stott, Can. J. Phys. **52**, 759 (1974).
[50]Y.-K. Park, J. T. Weber, M. Meshii, C. L. Snead, Jr., and C. G. Park, Phys. Rev. B **34**, 823 (1986).
[51]Y. Kong and K. G. Lynn (unpublished).
[52]N. W. Ashcroft and N. D. Mermin, *Solid State Physics* (Holt-Saunders, Philadelphia, 1981).
[53]R. W. Vook, Thin Solid Films **64**, 91 (1979).
[54]E. Bauer, in *The Chemical Physics of Solid Surfaces and Heterogeneous Catalysis,* edited by D. A. King and D. Woodruff (Elsevier, Amsterdam, 1984), Vol. 3B.
[55]A. Vehanen and J. Mäkinen, Appl. Phys. A **36**, 97 (1985).
[56]M. Debowska, R. Ewertowski, and W. Swiatkowski, Appl. Phys. A **36**, 47 (1985).